PHYSICS OF FLUIDS **27**, 021901 (2015)

Fog spontaneously folds mosquito wings

Andrew K. Dickerson,[1] Xing Liu,[1] Ting Zhu,[1,a)] and David L. Hu[1,2,a)]
[1]*School of Mechanical Engineering, Georgia Institute of Technology, Georgia 30332, USA*
[2]*School of Biology, Georgia Institute of Technology, Georgia 30332, USA*

(Received 29 October 2014; accepted 31 January 2015; published online 23 February 2015)

The flexibility of insect wings confers aerodynamic benefits, but can also present a hazard if exposed to fog or dew. Fog can cause water to accumulate on wings, bending them into tight taco shapes and rendering them useless for flight. In this combined experimental and theoretical study, we use high-speed video to film the spontaneous folding of isolated mosquito wings due to the evaporation of a water drop. We predict shapes of the deformed wing using two-dimensional elastica theory, considering both surface tension and Laplace pressure. We also recommend fold-resistant geometries for the wings of flapping micro-aerial vehicles. Our work reveals the mechanism of insect wing folding and provides a framework for further study of capillarity-driven folding in both natural and biomimetic systems at small scales. © *2015 AIP Publishing LLC.* [http://dx.doi.org/10.1063/1.4908261]

I. INTRODUCTION

Most studies have focused on insect flight in still, clean air. However, flying insects face turbulent air as well as harsh weather such as rainstorms, fog, and dew, and studies are beginning to examine how insects contend with such airborne contaminants.[1–4] In this study, we investigate the robustness of the mosquito wing (Figs. 1(a) and 2) under high humidity conditions. We discover that dew collection causes mosquito wings to spontaneously fold. Our findings may inspire more weather-resistant designs for the wings of flapping micro-aerial vehicles (MAVs).[5–9] Understanding this vulnerability of insect wings may help us find potential methods for pest control. Below, we review several aspects of the wing-folding process, from solid mechanics to fluid mechanics to biology.

Folding has long been a way to compact flat sheets, such as maps, for storage. Recent progress from both solid mechanics and computational origami has yielded greater understanding of the folding process, and a greater variety of materials to which folding can be applied. Technological innovations involving folding include solar panels of satellites, or the pleating to stiffen manufactured metal sheets. A canonical problem in this field is the problem of folding a flat sheet with a minimum of actions. The use of water drops has long been known to be a promising way to spontaneously fold small-scale structures. Such a method is known as "capillary origami."

Py *et al*. wrote one of the seminal papers in capillary origami, demonstrating the static folded shapes can arise from the emplacement of a water drop on both rectangular and triangular sheets.[10] The drop was fully encapsulated by the sheet for particular sheet geometries. The authors rationalize this spontaneous closure on the basis of capillary forces overcoming elastic forces within the sheet. A similar study by Fargette *et al*. investigates capillary-induced snap-through instabilities of millimetric beams, in which the beam's curvature becomes quickly reversed due to the placement of a drop.[11] Capillary forces, negligible at length scales associated with human locomotion, become dominant at the millimetric length scales of water drops. In order for capillary forces to overcome the elastic forces of the sheets, Fargette *et al*. specially fabricated thin polydimethylsiloxane (PDMS) sheets of 40-80 μm in thickness. In this study, we show that such encapsulated drops

a)Authors to whom correspondence should be addressed. Electronic addresses: hu@me.gatech.edu and ting.zhu@me.gatech.edu

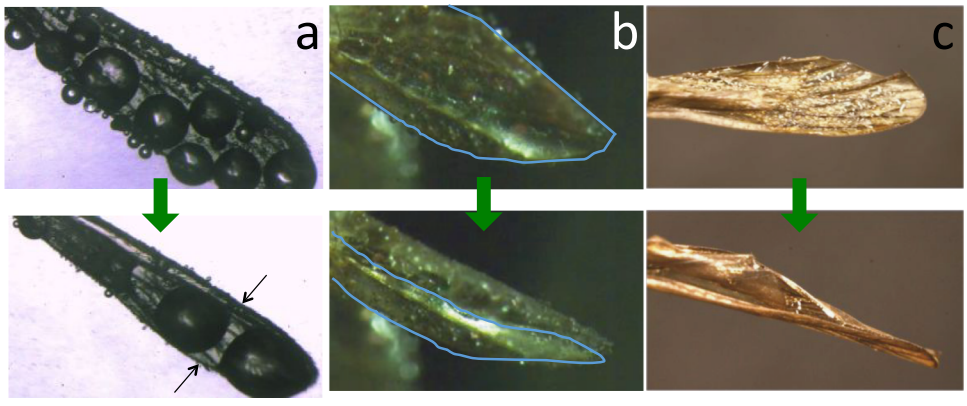

FIG. 1. Folding of wings belonging to a (a) mosquito, (b) fruit fly, and (c) stonefly. The blue outline in (b) traces wing edges of the fruit fly.

can also occur within natural materials such as insect wings. We also provide a robust theoretical method to calculate wing shapes.

Since the article by Py *et al.*, there have been a number of applications of this core principle of capillary origami towards variations in geometry and length scale. In micro-fabrication, folding can

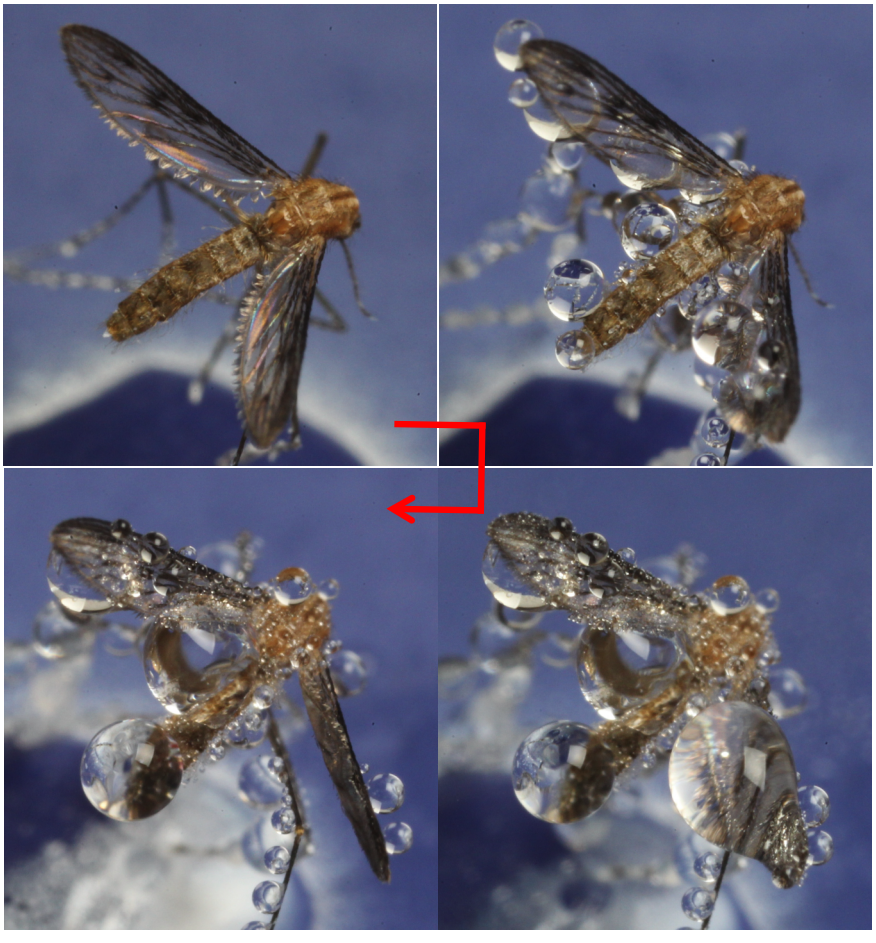

FIG. 2. Photographic sequence of a mosquito becoming increasingly wet due to exposure to fog. Ultimately, the bigger drops on the right wing fall way, leaving behind a tightly folding wing, unsuitable for flight.

produce three-dimensional structures from microscopic silicon sheets.[12] The capillary attraction of fluid menisci can be harnessed to provide large displacement, rotation and ultimately self-assembly of individual floating parts.[13] Floating biologically inspired flower-shaped structures have been used to encapsulate and then release fluid upon demand.[14] However, all these studies involve synthetic sheets, and few studies have begun to study capillary origami in nature.

Folding within the plant and animal kingdom can be categorized into both advantageous and disadvantageous. Examples of advantageous folding include the mimosa plant that folds for protection in response to touch, or the ladybug that folds its wings compactly for storage.[15–17] Leaves and wings are flexible and lightweight, which provide aerodynamic advantages, but also potential hazards. In wet conditions, the flexibility of these structures lead them to be easily folded.

To resist such capillary forces, insect wings and many plant surfaces have evolved hydrophobic, and often superhydrophobic, wetting properties. Super-hydrophobicity is imbued by a combination of a lipid layer and often surface microstructure,[18] which causes drops to spontaneously roll off and carry away contaminants. This ability is called self-cleaning.[19–22] Anisotropic surface structures, such as in butterfly wings, are known to cause drops to roll off in preferred directions.[18] Altering the surface structure via micro-scale contaminants, such as dust, or dissolution of the lipid layer, rapidly degrades their ability to stay clean and dry.

Pearl-shaped drops, such as those atop Lotus leaves, are the physical manifestation of a functioning super-hydrophobic surface. Drops much larger than the microstructures on the surface will exhibit a Cassie-Baxter wetting state such that the drop sits atop the structures with a thin layer of air underneath.[23] This Cassie-Baxter state is shown for a stonefly wing in Fig. 3(a). This is a favorable wetting state for the organism, allowing for easy drop removal. However, fog and dew drops can be comparable in size to the microstructures, and a groove-filling Wenzel-like behavior is observed, pinning drops to the surface and decreasing their mobility.[24] A Wenzel state induced by fog on an insect wing is shown in Fig. 3(b). Coalescence of drops on the wing can pin the fluid to the edge of the wing, generating a fold as shown in Fig. 3(c). This transition to a Wenzel state has been previously observed[25] in a number of systems, including the folding of small, hydrophilic

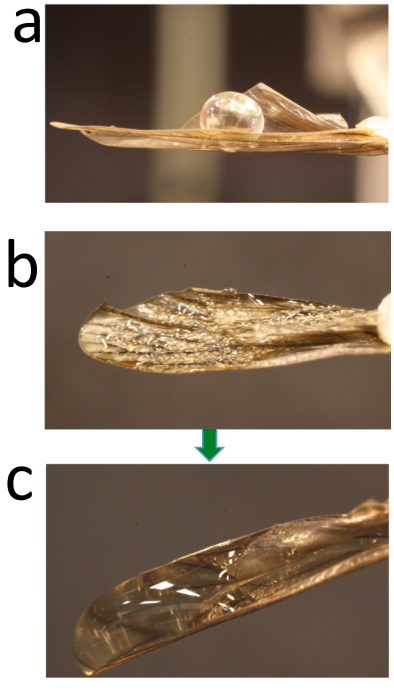

FIG. 3. Cassie, Wenzel, and folded states of a stonefly wing. (a) A dry wing is super-hydrophobic, with a contact angle ~ 150°. (b) Fog wets the wing upon contact, as shown by the small flat drops adhered to the wing. (c) Accumulation of water shows a drop of much lower contact angle ~ 50°. The wing also appears slightly folded due to associated capillary forces.

wings of *Schedorhinotermes* sp. termites which are poor flyers.[1] These termites fly after rainfall and never contact mobile drops. Instead, they so prefer hydrophilicity for colonization purposes, allowing them to remain trapped in areas where large amounts of moisture are present, allowing the termites to mate.

For membranes to fold, they must be sufficiently flexible. The stiffness of many natural membranes, including insect wings is heterogeneous and remains the topic of ongoing research. It is known that a wing's highly specialized structural properties are a key factor in the production of aerodynamic lift.[26] For example, bumblebees exhibited an 8.6% reduction in lift with stiffened wings. Insect wings are flexible and highly resilient due to the presence of the elastic protein,[27] resilin, which enables a wing to store mechanical potential energy when bent.[28] Resilin is also found in mobile wing joints, contributing to energy recovery and leading edge wing twisting.[29] In parallel, wings are purposefully stiff in certain regions, such as the leading edge.[30] A wing's veins provide resistance against aerodynamic bending moments[31] and create span-chord stiffness anisotropy. Stiffness in the spanwise direction is 1-2 orders of magnitude higher than in the chordwise direction.[32] Thus, insect wings are most likely to fold in the chordwise direction, like a hotdog. Finite element models based on *Manduca sexta* forewings show spatial variation in flexural stiffness, firming proximal regions, and allowing edges, where subtle changes in shape are critical to lift production, to bend.[30] Insects in the Coleoptera, or beetle, order possess wings that fold via complex patterns, allowing the wings to be stored below the outer shell when not in use.[16,17] Nevertheless, most insect wings are not designed to fold. Due to the highly specialized relationship between an insect's wing shape and flexural stiffness, it follows that drops can be quite hazardous to a wing's function. Attached drops can modify a wing's curvature, greatly increase a wing's mass, and affect the leading edge, which affects flight performance.

In this study, we investigate the self-folding of insect wings exposed to fog. Our experimental methods for insect handling and imaging are provided in Sec. II. We present our results in Sec. III, including a theoretical model that encapsulates the mosquito wing bending as a function of drop size. In Sec. IV, we present a discussion of our results and avenues for future work, and in Sec. V we provide closing remarks.

II. EXPERIMENTAL METHODS

A. Mosquito source and care

Male and female *Anopheles freeborni* mosquitoes are provided by the Centers for Disease Control (CDC) in Atlanta, GA. Mosquitoes are adults upon delivery and are fed a nectar solution prepared by the CDC. No attempt was made to separate the sexes in our experiments. Various other insects were wild-caught locally.

B. Deposition experiments

Dew particles are produced with an Air O Swiss 7145 consumer humidifier with continuous adjustability in fog density. A droplet sizing instrument (DC-III; KLD Labs Inc., New York) is used to characterize the spectra of droplets generated by our humidifiers. A hose attached to the humidifier directs the stream of mist to ablated wing. A Phantom V210 and Phantom Miro 110M high-speed camera are the primary tools for observance of wing folding, and we film over a range of 24–3 000 fps. The camera is attached to an Olympus SZX16 dissection microscope, using up to an 8x zoom. Ablated wings are lit with a single 1×3 LED array by Visual Instrumentation Corporation (Model 900 420) from above, and a Dedolight DT4.1 from below. The lights provide enough heat to evaporate deposited moisture within 10 min, but do not warp dry wings.

C. Wing measurements and preparation

Measurements of wing dimensions and wing cross-sectional shape within videos are done digitally with Tracker, an open source physics program. Drop areas are found by tracing the drops in

Tracker, creating an irregularly shaped polygon of more than 100 sides. The polygon's coordinates are exported to MATLAB for area calculation. Average wing thickness was measured with a micrometer. Such a method captures the thickness of the veins, but not necessarily that of the membrane.

To film the shape of mosquito wings, we ablated the wings by shortening the wing by roughly 1 mm from the tip, via a single cut in the chordwise direction. This cut permits us to film flat section of the wing, which reduces image blur when estimating drop shape and measuring D from side views of the wing.

III. RESULTS

A. Experiments

1. Experiments with isolated mosquito wings

In experiments with live mosquitoes, we observed exposure to fog would cause the wings to spontaneously fold, as shown in Fig. 2. To better film this phenomenon, the remainder of experiments in this study were performed with isolated wings freshly removed from live mosquitoes.

A consumer grade humidifier is used to emulate heavy fog conditions and nocturnal dewfall, producing a stream of 5–35 μm diameter droplets, with an average diameter of 15 μm. Individually, such droplets are too small to fold mosquito wings: specifically, the drops do not extend over a large enough length to overcome the bending stiffness of the wing, with a typical chord length of 0.7 – 1 mm. At the same time, sufficiently large drops that span the wing are also large enough that gravitational forces would cause the drop to roll from the wing. Thus, both very large and very small drops are ineffectual in folding wings; instead, intermediate-sized drops are the most hazardous.

Interestingly, Fig. 1 shows that intermediate-sized drops can be formed through coalescence of small fog drops deposited on the wing. Such coalescence occurs so quickly that the drop is wrapped by the wing before the drop has a chance to fall due to gravity. By wrapping the drop, the wing increases its contact perimeter with the drop, and with it, the folded capillary forces pinning the drop in place.

Before exposure to fog, drops exhibit a Cassie wetting state (Fig. 3(a)). After 3 s of exposure to a stream of fog particles, small droplets are observed scattered throughout the wing (Fig. 3(b)). These small droplets serve two functions for further water addition. First, they act as deposition sites and grow upon additional exposure to dewfall or fog particles. Second, they allow larger drops to stick to the wing. Once the wing has wet, a high-speed camera is needed to capture the sequence of shapes, shown in supplementary videos 1 and 2.[33] Folding occurs as drops coalesce across the span of the wing. This coalescence cascade creates a bigger drop pinned at the wing edges, whose positioning generates sufficient leverage to fold the wing.

Since drops deposit and coalesce haphazardly, the degree of folding is difficult to control in our experiments. Instead, many trials are used to demonstrate the variations possible on folding tightness. Fig. 1(a) shows a gently folded mosquito wing, with the drops still nearly spherical after the folding process. Fig. 1(b) shows a tight span-wise fold of a fruit fly wing. Blue outlines show the edges of the wing before and after folding. Fig. 1(c) shows a tight fold of a stonefly wing; such tight folds are difficult for the insect to unfold as they expose little of the drop, which decreases evaporation rate.

The mosquito wing's small size makes it intractable to measure elastic modulus. Instead, we measure the elastic moduli of stone fly, cicada, cockroach, and honey bee wings to determine a suitable value for analysis. Additionally, we assume vein size, composition, and pattern play no appreciable role in chordwise stiffness. In any case, we expect the elastic moduli mosquito wings to be at least of the same order of magnitude of similar flyers. The elastic modulus is measured by taking a chordwise section of each wing and using an analytical balance to measure the force required to slightly deform each wing. A video camera is used to measure the wing's deflection. We find the modulus E = 16 MPa (N = 2) for stone fly wings, $E = 25 \pm 5$ MPa (N = 3) for cicada wings, $E = 126 \pm 16$ MPa (N = 3) for cockroach wings, and E = 381 (N = 2) for honey bee wings. As an input for our model, we assume a mosquito wing elastic modulus of $E \approx 20$ MPa, by choosing soft

wings in the measured range. Our rough measurements of wing thickness and elasticity will be used as inputs to our numerical model.

2. Controlled wing folding through evaporation

To vary the size of the drop on the wing, we use humidifier fog to deposit and grow a large drop, and hot light coupled with cessation of fog to evaporate the drop. A camera points along the span of the wing and a series of snapshots are taken.

Fig. 4 shows the images of folded wings as the drop size continuously decreases by evaporation. We observe two distinctly different behaviors among the wings of different sizes. Fig. 4(a) shows a wing that forms a deeply folded shape and closes more tightly as the water drop evaporates, resulting in an abrupt and complete shut. In contrast, Fig. 4(c) shows a rare case where the wing retains its gently folded shape; the wing becomes more closed with evaporation of the water drop and reopens as the drop size decreases below a certain threshold.

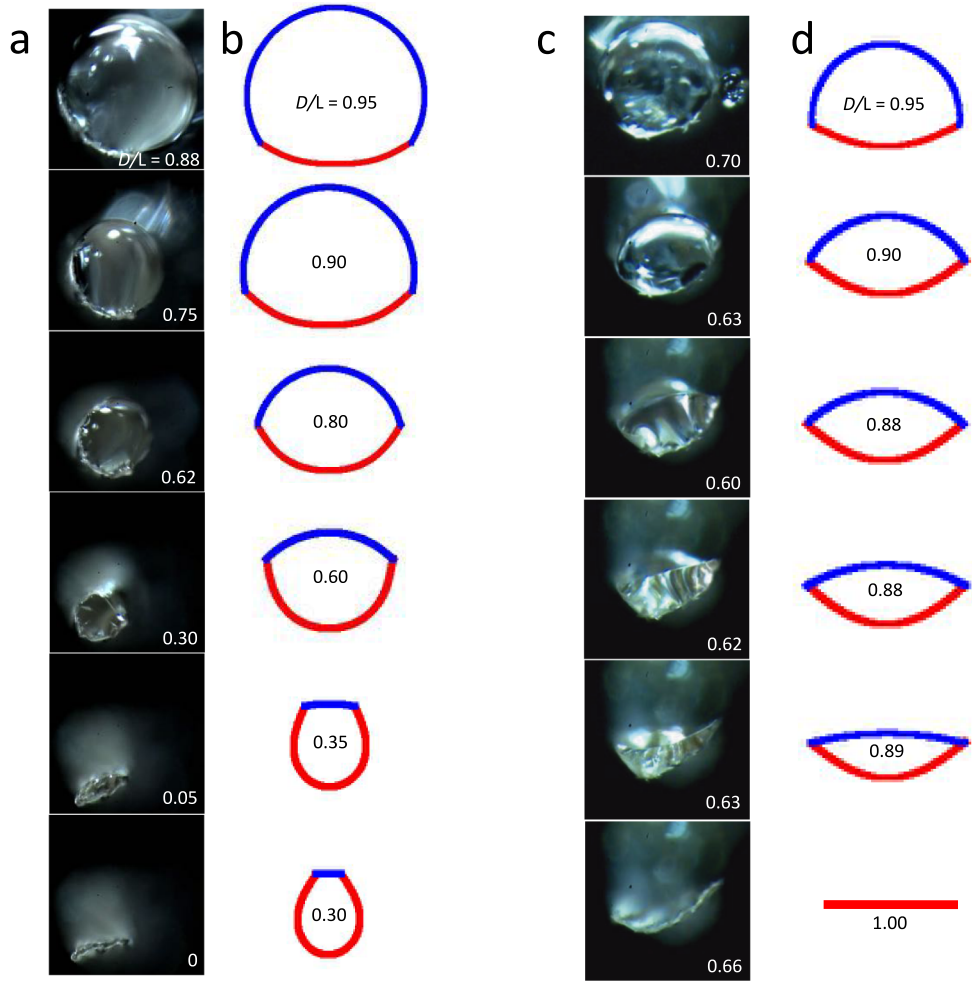

FIG. 4. Evaporation of water drops from two mosquito wings, whose behavior shows high sensitivity to wing stiffness. In (a), the wing closes tightly, from a dimensionless width of $D/L = 0.88$ to $D/L = 0$. In (b), assuming an elastocapillary length $L_{EC} = 150\ \mu$m, simulations show a qualitatively similar behavior, from $D/L = 0.95$ to $D/L = 0.30$, the range of our computations. In (c), evaporation of the drop causes the wing to remain open at $D/L \approx 0.70$. In (d), simulations using a stiff mosquito wing, with $L_{EC} = 250\ \mu$m, shows a qualitatively similar behavior for an initial $D/L \approx 1.0$. In (a)-(d), the experiments and simulation are most closely matching for small D/L. For large D/L, our simulations under-predict the drop area A for a given D/L.

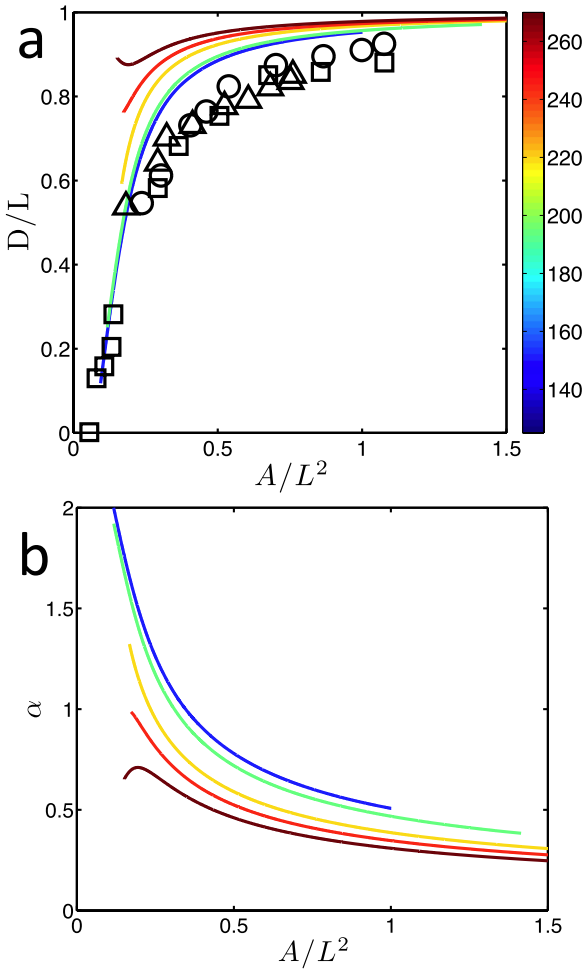

FIG. 5. Deformation of the wing as a function of drop size. (a) Experimental points and theoretical curves of wingtip extent D/L in relation to drop area A/L^2. (b) Theoretical curves of wingtip angle α in relation to drop area A/L^2.

To quantify the folded geometries, we measure both the cross-sectional area A of the drop and the wing edge-to-edge distance D, the former of which is considered as the equivalent measure of drop volume in our two-dimensional model discussed in Sec. III C. Experiments, which take 7 – 10 min, are performed on an ablated mosquito wing, where the wing is cut near its tip in order to facilitate measuring D from side views of the wing. Through this process, we obtain controlled folding of the insect wing that can be directly compared with our theoretical predictions. Fig. 5(a) shows the measured wing distance D (normalized by the wing arc length L) versus the area of the drop A (normalized by L^2) for three mosquito wings. Each open symbol represents a different wing, and trends are reasonably consistent among the three wings tested, which correspond to the case of deep folding shown in Fig. 4(a). As the drop evaporates, A decreases and the wing closes more tightly, thus reducing D. When the wing folds very tightly ($D/L < 0.4$), the drop volume has become so small that the meniscus falls below the line drawn between wing edges (dashed-dotted line in Fig. 6). Below the smallest drop area A/L^2 measurable of 0.1, the wing shuts completely, wherein $D = 0$. Conversely, as the drop increases in volume, the wing unfolds, nearly reaching the flat wing distance of $D = L$.

B. Scaling

Before detailed description of model, it is instructive to analyze the capillarity-driven folding by scaling considerations. The insect wing is approximated as an elastic membrane. Folding of such

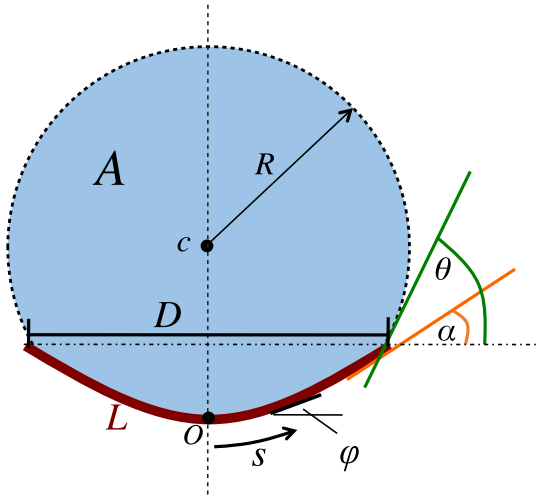

FIG. 6. Schematic of a water drop folding a two-dimensional wing. The drop is circular with a radius R and center point C. The angle α is the rotation angle of the beam end with respect to the horizontal. The angle θ is measured between the line tangent to the free water surface and the horizontal. Note that θ is distinct from the equilibrium contact angle.

elastic membrane wing by a liquid drop is dictated by the competition of capillary forces and elastic bending. Fig. 6 shows a simplified two-dimensional representation of an insect wing as an elastic beam with a characteristic length of L. The beam is covered by a single drop of radius R pinned to the edge of the beam. The bending of the beam, on one hand, reduces the liquid-air area of the drop A and thus the surface energy $U_s \sim \sigma A \sim \sigma\pi R$, where σ is the surface tension of the drop. On the other hand, the bending deformation increases the elastic energy of the beam $U_e \sim EI\kappa^2 R$, where E is Young's modulus and $I = t^3/12$ is the area moment of inertia per unit wingspan. Here, we assume that the arclength L of the curved beam, as well as its radius of curvature $1/\kappa$, scale with the drop radius R. The surface and bending energy are comparable when the length scale R of the beam is

$$L_{\mathrm{EC}} = \sqrt{\frac{EI}{\sigma}}, \tag{1}$$

a parameter known as the elastocapillary length.[10] The minimal limit for size of sheet which will fold is governed by the elastocapillary length L_{EC}. This length scale, as shown in Eq. (1), scales as the sheet thickness $t^{3/2}$. Therefore, thinner membranes produce tighter folds[10] and the thickest membranes cannot fold.

C. Modeling

A two-dimensional fluid-structure model is developed to study the mechanics of folding of an elastic beam driven by the capillary force from a single drop. In light of the energetics of folding in Sec. III B, we consider only the elastic bending and capillary tension, and ignore the gravitational force. Fig. 6 shows the schematic of a drop-beam pair. The shaded drop is bounded above by its free surface (dashed line) and below by the beam (solid line). Large deflection of the beam during folding necessitates the use of the classic Euler elastica theory. In this theory, the convenient kinematic variable is chosen as the angle of rotation of the beam $\varphi(s)$ relative to the horizontal axis, where s is the curvilinear coordinate along the beam, with $s = 0$ at the lowest point of the beam and $s = L/2$ at the rightmost point; due to symmetry, we consider only one half of the beam.

The equilibrium equation can be derived from the moment balance at a differential beam element. That is, the internal bending moment in the beam element is $M = EI\kappa$, where $\kappa = \mathrm{d}\varphi/\mathrm{d}s$. This moment is related to the distributed force P acting on the beam according to $P = \mathrm{d}^2M/\mathrm{d}s^2$. As shown in Fig. 6, the beam is subjected to the pressure in the liquid drop, which satisfies Young-Laplace's equation $P = -\sigma/R$. Combination of the aforementioned moment and pressure

relations yields

$$EI\frac{\mathrm{d}^3\varphi}{\mathrm{d}s^3} = -\frac{\sigma}{R}, \quad s \in \left[0, \frac{L}{2}\right]. \tag{2}$$

Solving Eq. (2) requires three boundary conditions. First, we consider the shear force at the end of the beam. At $s = L/2$, the internal shear force in the beam is given by $dM/ds = EId^2\varphi/ds^2$, while the external shear force is the resolved component, normal to the beam, of the surface tension from the liquid drop. Balance of the two shear forces yields a boundary condition of

$$EI\frac{\mathrm{d}^2\varphi}{\mathrm{d}s^2} = -\sigma\sin(\theta - \alpha), \text{ at } s = \frac{L}{2}, \tag{3}$$

where the angles θ and α represent the angle of drop surface and the beam, respectively, with respect to the horizontal. The contact angle is insignificant at the beam's edges because the beam is elastically deformable. If the elastic rigidity of the beam were to increase, the beam would become flattened and the angle α would approach zero. In the limit of $\alpha = 0$, θ reduces to the contact angle of a drop pinned at the end of a flat, rigid beam. The angle α can also be represented by the beam's angle of rotation φ at the edge of the beam $s = L/2$. Another boundary condition is given by zero external moment at the end of the beam, resulting in

$$\frac{\mathrm{d}\varphi}{\mathrm{d}s} = 0, \text{ at } s = \frac{L}{2}. \tag{4}$$

In addition, the symmetry of the beam imposes a constraint at its midpoint, giving the third boundary condition

$$\varphi = 0, \text{ at } s = 0. \tag{5}$$

From the above equilibrium equation and boundary conditions, we obtain the theoretical solution of $\varphi(s)$. The input for numerical solutions involves the wing's chord length L and thickness t, as well as the surface tension of the drop σ. The elastocapillary length is also given as an effective measure of the bending stiffness (per unit wingspan) $B = EI$ of the beam.

1. Numerics

The equilibrium geometries of a bent beam are solved by numerical integration, based on Eqs. (2)–(5). With the boundary conditions of Eqs. (3)–(5), triple integration of Eq. (2) yields

$$\varphi = -\frac{1}{6}\frac{\kappa_w}{L_{\mathrm{EC}}^2}s\left[s^2 + \lambda\frac{L}{2}s - \left(\frac{3}{4} + \frac{\lambda}{2}\right)L^2\right], \tag{6}$$

where $\kappa_w \equiv 1/R$, and λ is a dimensionless parameter that satisfies the following implicit equation:

$$\lambda = \frac{6\sin(\theta - \alpha)}{\kappa_w L} - 3, \tag{7}$$

where both θ and α are dependent on λ. To solve Eq. (6), the required inputs include L and L_{EC}.

Equation (6) can be normalized as

$$\varphi = -\frac{1}{48}\frac{L^3}{L_{\mathrm{EC}}^2}\kappa_w\eta(\eta^2 + \lambda\eta - 3 - 2\lambda), \tag{8}$$

where $\eta \equiv 2s/L$ and $\eta \in [0, 1]$. The iteration variable for convergence is λ. To satisfy the condition in Eq. (7), a fixed point algorithm is used considering the dependence of θ and α on λ. To speed up the convergence, Steffensen's method[34] is employed such that

$$\begin{aligned} \lambda^* &= f(\lambda^n), \\ \lambda^{**} &= f(\lambda^*), \\ \lambda^{n+1} &= \lambda^n - \frac{(\lambda^* - \lambda^n)^2}{\lambda^{**} - 2\lambda^* + \lambda^n}, \end{aligned} \tag{9}$$

where $f(\lambda) = 6\sin(\theta - \alpha)/(\kappa_w L) - 3$.

The solution of Eq. (8) is used to numerically determine the relation between the edge-to-edge distance of the bent beam D and the drop area A, which are defined, respectively, as

$$\frac{D}{L} = \int_0^1 \cos(\varphi(\eta))\, d\eta, \tag{10}$$

$$\frac{A}{L^2} = \tilde{R}^2(\pi - \theta + \sin\theta\cos\theta) - \frac{1}{2}\int_0^1 \cos(\varphi(\xi)) \int_1^{\xi} \sin(\varphi(\eta))\, d\eta d\xi, \tag{11}$$

where $\tilde{R} = R/L$ is the normalized radius of water drop.

Since numerical integration is performed over a wide range of folded geometries, care has to be taken regarding the limits of α and θ as defined in Fig. 6. By definition, $\alpha = \varphi|_{\eta=1}$, such that $\alpha = 0$ corresponds to a flat wing and $\alpha = \pi/2$ a completely folded wing. However, different formulas need to be used to evaluate the associated θ as the center of the circular drop crosses the line joining the two edges of the beam. In the case where the center of the circular drop is above this line, $\theta = \pi - \arcsin(D/2R)$ (Fig. 6), while $\theta = \arcsin(D/2R)$ in the case where the center lies below the line (Fig. 6). We find solutions for A and D for each case separately, and combine them to give a complete theoretical prediction.

D. Theory predicts sequence of folded wing shapes

In this section, we compare our model predictions to experimental results. Our model can predict the sequence of bending shapes of the wing, given the volume of the drop and measurements of wing thickness and elasticity. We measure a mosquito wing to have a thickness of $t \sim 10$ μm, and assume it has Young's modulus of $E \sim 20$ MPa, similar to that of a cicada and stonefly wings. Thus, the wing stiffness per unit wingspan is $B = EI = Et^3/12 = 1.7 \times 10^{-9}$ N m. The corresponding elastocapillary length for this stiffness is $L_{EC} = 150$ μm, which we will use in our numerics. Considering a mosquito wingspan of $S = 2$ mm, the stiffness $B^* = BS = 3.4 \times 10^{-12}$ N m^2 is at least not greater than those measured by previous investigators ($B^* < 10^{-8}$ N m^2 for wings with $L < 1$ mm).[35] The discrepancy is likely due to previous investigators' experimental difficulty in measuring wing stiffness of the smallest insects. Nevertheless, we proceed with using our estimation of B and L_{EC} in our model.

Using this value of $L_{EC} = 150$ μm for mosquito wings, our modeling results capture the folding behaviors in experiments. The plots in Fig. 4(b) show the numerical solutions of a bent beam covered with a drop of different volumes (i.e., areas of A). Juxtaposed with these plots are experimental images of the beam at different folded extents, ranging from a nearly flat beam corresponding to $D/L \approx 1$ to a beam bent in half, corresponding to $D/L \approx 0.3$.

When the drop is large, there is only one type of equilibrium solution, giving a bent beam with a shallow fold, as shown by the first plots in Figs. 4(b) and 4(d) corresponding to $D/L \approx 1$. In contrast, when the drop is small, there are two types of equilibrium solutions, depending on the bending stiffness of the beam B. That is, for a soft beam with a stiffness of that of a mosquito wing, such that $L_{EC} = 150$ μm, the drop is wrapped by the largely bent beam that develops a deeply folded geometry, shown in Figs. 4(a) and 4(b). The behavior changes drastically, upon consideration of a beam with double the stiffness, such that $L_{EC} = 250$ μm, as shown in Figs. 4(c) and 4(d). Such a beam retains its shallow fold as the drop size decreases.

To facilitate a direct comparison between experiment and modeling, we also calculate the relation between the edge-to-edge distance D of the wing and the cross-sectional area A of the drop, both of which can be obtained by numerical integration once the folded geometry is determined by $\varphi(s)$. In Fig. 5(a), the solid lines represent our modeling predictions of D versus A, with different values of the elastocapillary length L_{EC} represented by line color. Thus, elastocapillary length L_{EC} is shown as a free parameter. The blue and green curves correspond to the case of soft beams in Figs. 4(a) and 4(b), with the characteristic values of $L_{EC} = 125 - 200$ μm.

In Fig. 5, this stiffness of the mosquito wing yields the sequence of wings shapes given by the dark blue trend line, which closely fits our experimentally measured sequence of folded wing shapes. We thus conclude that our model is physically realistic, as it provides consistency between

mosquito wing properties and sequence of folded shapes. We note that the consistency is best for small drops. As drops increase in size, our experiments generally give a 10% higher degree of folding than predicted.

The brown and red lines in Fig. 5(a) correspond to the case of stiff beams in Fig. 4(d), with $L_{EC} > 250$ μm. In this case, a stiff beam retains its shallow folded geometry. Interestingly, the wing becomes more closed as the drop-size decreases, and reopens as the drop areas become less than $A = 0.2$. Such anomalous re-opening behavior has been observed in our experiment, Fig. 4(c), suggesting that a fraction of mosquitoes can have wing stiffnesses for which $L_{EC} > 250$ μm.

From the biological standpoint, such resistance to folding indicates that certain breeds of mosquitoes have natural variations in their thickness or material properties. Specifically, our numerical results show that a mosquito that changes its L_{EC} from 150 to 250 can avoid folding. Physically, this change is associated with a doubling of elastic modulus, or equivalently an increase in wing thickness by 25%, both of which seem reasonable, given the large number and range in habitats of species of mosquitoes.

To further appreciate the extreme shape change during folding, we plot in Fig. 5(b) the calculated values of the beam's angle α with respect to the horizontal, defined schematically in Fig. 6. The same parameter of L_{EC} is assigned for the blue and green curves in Figs. 5(a) and 5(b). As the drop size decreases, α increases from 0.5 to 1.5 radians, i.e., from an acute to obtuse angle, passing $\pi/2$. The span of such a wide range of α with decreasing drop size coincides with the change from a shallow to a deeply folded geometry of the soft beam, as shown in Figs. 4(a) and 4(b).

IV. DISCUSSION

In our study, we have considered the mechanics of an elastic insect wing folded by the capillary forces associated with an evaporating drop. With mosquito wings, we noticed a systematic error of 10%, likely arising due to various simplifications invoked in our model of the membrane wing, liquid drop and their interactions.

In our model, we simplify a three-dimensional folding process to a two-dimensional one. In general, this cannot be done, because of the variance in wing properties among insects. For instance, in supplementary video 1,[33] fruit fly wings fold in the spanwise direction due to three-dimensional drop effects. However, a mosquito wing's long shape and stiffness anisotropy justify our use of a 2-D model. As can be seen in Fig. 2, the mosquito wing is long and thin, causing drops to be sausage-shaped (large span length, small chord length). Thus, the drop's chordwise radius of curvature is considerably smaller than its spanwise radius of curvature. The chordwise capillary forces are therefore dominant, causing the wing to fold accordingly.

Two-dimensional modeling is further justified by the wing's anisotropic bending stiffness, a common property among flying insects. In particular, veins in wings provide resistance against aerodynamic bending moments,[31] creating span-chord stiffness anisotropy. Stiffness in the spanwise direction is 1-2 orders of magnitude higher than that in the chordwise direction,[32] indicating a wing should fold more easily in the chordwise direction, as shown in Fig. 3(c).

We study a drop pinned at the wing edge, corresponding to a case where the drop size is comparable to the chord of the wing. In this scenario, the contact angle at the wing edge is determined by a force balance between the surface tension of the liquid drop and the bending force at the wing tip. This local equilibrium condition is given by Eq. (3) and enforced in our numerical calculations. On the other hand, a related problem involves the study of dynamics of drop spreading or shrinking, which requires the detailed characterization of a free contact line and accordingly a variable contact angle at the drop edge. However, such problem is important only when the drop size is smaller than the span of the wing. It has been studied by earlier theoretical works (e.g., Neukirch *et al.*[36]). Albeit interesting, this problem is not within the scope of our study.

Our consideration of a large drop permitted us to neglect the surface properties of the wings, which must be considered for smaller drops. Surface properties influence the transient nature of drop formation and coalescence. For example, butterfly wings are known to have surface anisotropy,[18] which may lead to drops migrating to the edge of the wing after multiple coalescence events.

However, once a drop is formed and pinned to the wing's edges, the surface properties of the wings play less of an effect.

Antkowiak *et al*. have shown that drop impact can also give rise to drop encapsulation.[37] In our model, we did not consider drop inertia. In nature, however, a wet wing can be struck by high-speed drops such as those during rainstorms.[3] Furthermore, drops falling from wings can help to induce folding. In fact, in Fig. 2, the wing is tightly folded to a drop that has become large and then dripping from the wing. Thus, wet wings can be induced to fold in other ways than pure accumulation as considered in this study.

Although this study focused on mosquitoes, we also observed the isolated wings of other insects when subjected to humidifier fog. Insects wings of thickness less than 50 μm, such as seen on fruitflies, fireflies, lacewings, forage looper moths, and stoneflies, are susceptible to folding. Wings of thickness $75-95$ μm, such as those of honeybees, bumblebees, cicadas, and cockroaches, are too stiff to fold via capillary forces. Wing folding occurred among nine of thirteen species observed, suggesting that it may be a widespread phenomenon. Experiments with live insects should be conducted to determine if such folding is indeed so widespread. Indeed, even mosquitoes will exhibit behaviors to remove drops such as flapping their wings or falling in mid-flight.[2]

V. CONCLUSION

We investigate the spontaneous folding of insect wings due to exposure to fog. Fog causes an insect's water-repellent wings to become wet. As water continues to accumulate, a series of drop coalescences occur that increase the size and span of the drops, providing the largest drops with sufficient leverage to fold the wing in the chordwise direction. Wings can become so tightly folded that they require long times to dry, during which they are unusable for flight.

In our study, we also report new theoretical methods for solving fluid-solid interaction problems. We solve for the shape of a folded wing by modeling the wing as an elastica. Our model demonstrates that an insect wing is most endangered from a cycle of water accumulation and then evaporation. A large volume of water is needed initially to increase the moment arm applied by the drop. However, this large volume generates only a shallow fold of the wing. Subsequent evaporation is required for a wing to generate a deep fold. Our work reveals the mechanical underpinnings of fold growth in mosquito wings, and provides a physical basis for further study and control of the capillary-driven folding in micro-technology applications.

ACKNOWLEDGMENTS

We thank Sam Beadles, Courtney Clement, and Hyun Choe for early contributions, and NSF (PHY-0848894) for support.

[1] G. S. Watson, B. W. Cribb, and J. A. Watson, "Contrasting micro/nano architecture on termite wings: Two divergent strategies for optimising success of colonisation flights," PLoS One **6**, e24368 (2011).
[2] A. K. Dickerson and D. L. Hu, "Mosquitoes actively remove drops deposited by fog and dew," Integr. Comp. Biol. **42**, 1–6 (2014).
[3] A. Dickerson, P. Shankles, N. Madhavan, and D. Hu, "Mosquitoes survive raindrop collisions by virtue of their low mass," Proc. Natl. Acad. Sci. **109**, 9822–9827 (2012).
[4] A. K. Dickerson, P. G. Shankles, and D. L. Hu, "Raindrops push and splash flying insects," Phys. Fluids **26**, 027104 (2014).
[5] R. Wood, "The first takeoff of a biologically inspired at-scale robotic insect," IEEE Trans. Rob. **24**, 341–347 (2008).
[6] P. Zdunich, D. Bilyk, M. MacMaster, D. Loewen, J. DeLaurier, R. Kornbluh, T. Low, S. Stanford, and D. Holeman, "Development and testing of the mentor flapping-wing micro air vehicle," J. Aircr. **44**, 1701–1711 (2007).
[7] F. Van Breugel, Z. Teoh, and H. Lipson, "A passively stable hovering flapping micro-air vehicle," in *Flying Insects and Robots* (Springer, 2009), pp. 171–184.
[8] M. Groen, B. Bruggeman, B. Remes, R. Ruijsink, B. Van Oudheusden, and H. Bijl, "Improving flight performance of the flapping wing MAV delfly ii," in *International Micro Air Vehicle Conference and Flight Competition* (Delft University of Technology, Braunschweig, Germany, 2010).
[9] G. De Croon, K. De Clercq, R. Ruijsink, B. Remes, and C. De Wagter, "Design, aerodynamics, and vision-based control of the DelFly," Int. J. Micro Air Veh. **1**, 71–97 (2009).
[10] C. Py, P. Reverdy, L. Doppler, J. Bico, B. Roman, and C. Baroud, "Capillary origami: Spontaneous wrapping of a droplet with an elastic sheet," Phys. Rev. Lett. **98**, 156103 (2007).

[11] A. Fargette, S. Neukirch, and A. Antkowiak, "Elastocapillary snapping: Capillarity induces snap-through instabilities in small elastic beams," Phys. Rev. Lett. **112**, 137802 (2014).
[12] J. van Honschoten, J. Berenschot, R. Sanders, L. Abelmann, N. Tas, and M. Elwenspoek, "Fabrication of three-dimensional microstructures using capillary forces," in *Proceedings of the 20th Micromechanics Europe Workshop*, *(MME 09)* (Laas-CNRS, Toulouse, France, 2009), pp. 1–4.
[13] M. Boncheva, D. A. Bruzewicz, and G. M. Whitesides, "Millimeter-scale self-assembly and its applications," Pure Appl. Chem. **75**, 621–630 (2003).
[14] S. Jung, P. Reis, J. James, C. Clanet, and J. Bush, "Capillary origami in nature," Phys. Fluids **21**, 91–110 (2009).
[15] J. Braam, "In touch: Plant responses to mechanical stimuli," New Phytol. **165**, 373–389 (2005).
[16] W. M. Forbes, "How a beetle folds its wings," Psyche **31**, 254–258 (1924).
[17] F. Haas and R. G. Beutel, "Wing folding and the functional morphology of the wing base in coleoptera," Zoology **104**, 123–141 (2001).
[18] Y. Zheng, X. Gao, and L. Jiang, "Directional adhesion of superhydrophobic butterfly wings," Soft Matter **3**, 178–182 (2007).
[19] T. Wagner, C. Neinhuis, and W. Barthlott, "Wettability and contaminability of insect wings as a function of their surface sculptures," Acta Zool. **77**, 213–225 (1996).
[20] S. H. T. Nguyen, H. K. Webb, J. Hasan, M. J. Tobin, R. J. Crawford, and E. P. Ivanova, "Dual role of outer epicuticular lipids in determining the wettability of dragonfly wings," Colloids Surf., B **106**, 126–134 (2013).
[21] D. Byun, J. Hong, J. H. Ko, Y. J. Lee, H. C. Park, B.-K. Byun, and J. R. Lukes, "Wetting characteristics of insect wing surfaces," J. Bionic Eng. **6**, 63–70 (2009).
[22] M. Sun, G. S. Watson, Y. Zheng, J. A. Watson, and A. Liang, "Wetting properties on nanostructured surfaces of cicada wings," J. Exp. Biol. **212**, 3148–3155 (2009).
[23] J. Jopp, H. Grüll, and R. Yerushalmi-Rozen, "Wetting behavior of water droplets on hydrophobic microtextures of comparable size," Langmuir **20**, 10015–10019 (2004).
[24] T. Yu, J. Park, H. Lim, and K. Breuer, "Fog deposition and accumulation on smooth and textured hydrophobic surfaces," Langmuir **28**, 12771–12778 (2012).
[25] J. W. M. Bush, D. L. Hu, and M. Prakash, "The integument of water-walking arthropods: Form and function," in *Insect Mechanics and Control: Advances in Insect Physiology* (Elsevier, 2007), Vol. 176, pp. 117–192.
[26] A. M. Mountcastle and S. A. Combes, "Wing flexibility enhances load-lifting capacity in bumblebees," Proc. R. Soc. B **280** (2013).
[27] J. Gosline, M. Lillie, E. Carrington, P. Guerette, C. Ortlepp, and K. Savage, "Elastic proteins: Biological roles and mechanical properties," Philos. Trans. R. Soc., B **357**, 121–132 (2002).
[28] F.-O. Lehmann, S. Gorb, N. Nasir, and P. Schützner, "Elastic deformation and energy loss of flapping fly wings," J. Exp. Biol. **214**, 2949–2961 (2011).
[29] S. N. Gorb, "Serial elastic elements in the damselfly wing: Mobile vein joints contain resilin," Naturwissenschaften **86**, 552–555 (1999).
[30] S. Combes and T. Daniel, "Flexural stiffness in insect wings ii. Spatial distribution and dynamic wing bending," J. Exp. Biol. **206**, 2989–2997 (2003).
[31] A. B. Kesel, U. Philippi, and W. Nachtigall, "Biomechanical aspects of the insect wing: An analysis using the finite element method," Comput. Biol. Med. **28**, 423–437 (1998).
[32] S. Combes and T. Daniel, "Flexural stiffness in insect wings I. Scaling and the influence of wing venation," J. Exp. Biol. **206**, 2979–2987 (2003).
[33] See supplementary material at http://dx.doi.org/10.1063/1.4908261 for folding videos. **Video S1** shows folding sequences of a mosquito, fruit fly, and house fly wings, respectively, upon exposure to a fog stream. Folding generally occurs chordwise, tending to make the wings into hot-dogs. **Video S2** show a drop evaporating from the tip of two mosquito wings. Upon evaporation, the first wing closes more tightly, while the second returns to its natural shape.
[34] L. Johnson and D. Scholz, "On Steffensen's method," SIAM J. Numer. Anal. **5**, 296–302 (1968).
[35] J. Shang, S. Combes, B. Finio, and R. Wood, "Artificial insect wings of diverse morphology for flapping-wing micro air vehicles," Bioinspiration Biomimetics **4**, 1–6 (2009).
[36] S. Neukirch, A. Antkowiak, and J.-J. Marigo, "The bending of an elastic beam by a liquid drop: A variational approach," Proc. R. Soc. A (published online 2013).
[37] A. Antkowiak, B. Audoly, C. Josserand, S. Neukirch, and M. Rivetti, "Instant fabrication and selection of folded structures using drop impact," Proc. Natl. Acad. Sci. **108**, 10400–10404 (2011).